Processing and Application of Ceramics 12 [3] (2018) 240–247
https://doi.org/10.2298/PAC1803240S

Nanocrystalline composites in TiO_2 and SnO_2 system for ammonia resistance sensors

Anna Szczygielska[1,*], Zbigniew Pędzich[1], Wojciech Maziarz[2]

[1]*AGH - University of Science and Technology, Faculty of Materials Science and Ceramics, Department of Ceramics and Refractory Materials, Mickiewicza 30, 30-059 Krakow, Poland*
[2]*Institute of Metallurgy and Materials Science of Polish Academy of Sciences, Reymonta 25, 30-059 Krakow, Poland*

Received 10 April 2018; Received in revised form 11 July 2018; Accepted 11 August 2018

Abstract

This work describes the production of nanocrystalline TiO_2 and SnO_2 oxides, as well as their nanocomposites (containing 26.9, 58.7 and 79.0 wt.% of SnO_2) with two-stage sol-gel method combined with high temperature treatment. The phase composition and medium size crystallites were determined using X-ray diffraction analysis (XRD) and revealed that the nanocomposites crystallize in tetragonal structures of TiO_2 - anatase and SnO_2 - cassiterite. Specific surface area of the nanopowders, measured using sorption method (BET), changed from 42.1 to 160.8 m^2/g. The morphology of the nanopowders was observed using transmission electron microscope (TEM). As indicated by TEM images, the manufactured nanopowders were well crystallized and consisted of small, spherical grains. The obtained nanopowders were also tested for NH_3 gas detection application. The presented method of nanopowders synthesis enables to obtain nanocrystalline TiO_2 and SnO_2 oxides, as well as composites from TiO_2-SnO_2 of known and controlled chemical and phase composition. It also enables to obtain composites used for gas sensors. The sensor made of composite containing 58.7 wt.% of SnO_2 exhibited the best NH_3 sensing features.

Keywords: *nanocomposites TiO_2-SnO_2, nanopowders, sol-gel method, NH_3 sensors*

I. Introduction

The most commonly used sensors for gas detection are resistance gas sensors. In these sensors, the gas reacts with the sensor material, changing its electrical properties. Sensors consist of receptor and transducer element, substrate material, electrodes, heater, and can also be equipped with filters or other elements facilitating their operation [1]. The receptor element is composed of a chemically sensitive material, which changes its electrical conductivity during the gas reaction and thus allows gas detection. The most commonly used materials for construction of receptor and transducer elements are semiconductor oxide materials. If there is an oxidizing gas in tested atmosphere, the resistance of sensor material, which is an n-type semiconductor, increases, while in the presence of reducing gases it decreases [1–3]. Detection mechanism may be more complex when there are two opposing processes taking place, e.g. in case of ammonia detection (decrease in resistance due to the presence of ammonia and rise due to the formation of NO_x) [4,5].

The mechanism of operation of resistive gas sensors will be discussed on the example of chemisorption of oxygen, which can be adsorbed as O_2^-, O^- or O^{2-} (depending on energy, other ions will be dominant in the surface coverage). At room temperature, it takes the form of O^{2-}, whereas that of O^- is at higher temperatures. Oxygen is adsorbed on the surface (bound with oxygen vacancies present in the material) involving one or two electrons. Adsorption causes the electrons to detach from the donor level of the material, resulting in a formation of sites deprived of electrons or positively-charged sites close to the surface. As a result, an electron-depleted layer forms on the surface, leading to (decreased conductivity) higher resistance in

*Corresponding authors: tel: +48 12 617 24 96,
e-mail: *amarzec@agh.edu.pl* (A. Szczygielska)
pedzich@agh.edu.pl (Z. Pędzich)
w.maziarz@imim.pl (W. Maziarz)

an n-type semiconductor. An increase or a decrease in the oxygen ion concentration results in signal formation [6,7]. Chemisorption of oxygen can be presented as the following equation [8]:

$$\frac{\gamma}{2}O_2^{gas} + \alpha e^- + S' \rightleftharpoons O_{\gamma S}^{-\alpha} \quad (1)$$

where O_2^{gas} is oxygen molecule in the surrounding atmosphere, e^- is electron that can reach the surface, S' is location of oxygen chemisorption, α and γ are forms of oxygen ($\alpha = 1$ for singly-ionised forms, $\alpha = 2$ for doubly-ionised forms, $\gamma = 1$ for atomic forms and $\gamma = 2$ for molecular forms).

Where the surface reacts with a reductive gas, the amount of adsorbed oxygen is lower, resulting in an adequate number of electrons released to the conduction band. The higher the electron concentration in the conduction band, the greater the conductivity of an n-type semiconductor. Thus, if there is a reductive gas in the examined atmosphere, resistance of an n-type semiconductor sensor material is lower [6,7]. Chemisorption of a reductive gas as a reaction of it with the adsorbed oxygen on the sensor surface is described in the example of hydrogen in the following equation [8]:

$$O_{\gamma S}^{-\alpha} + \gamma H_{2(g)} \rightleftharpoons \gamma H_2O_{(g)} + \alpha e^- \quad (2)$$

where $O_{\gamma S}^{-\alpha}$ is form of adsorbed oxygen and e^- is electron capable of migrating to the surface.

It was also observed that as a result of the effect of two above-described types of gas, the electrical resistance (R) of any reductive gas sensor can be expressed as [8]:

$$R \propto p_{gas}^{-m} \quad (3)$$

where p_{gas} is molecular pressure of the reductive gas and m is coefficient specific for a given type of gas.

Ammonia gas is extremely dangerous to human health, and its detection constitutes a challenge for environmental, automotive and chemical industry as well as the medical diagnostics. The threshold limit value (TLV) for ammonia is 25 ppm. TLV of a chemical substance is believed to be a level to which a worker can be exposed day after day for a working lifetime without adverse effects. Whereas immediately dangerous to life and health (IDLH) value is 300 ppm. Ammonia possesses a threat to both the animals and agricultural workers in livestock facilities. Ammonia is a significant respiratory hazard for workers who experience long-term exposure to this gas in constant average values greater than 25 ppm. Therefore, research on the creation of sensors with different requirements regarding the detection limit, reaction time and temperature range is still underway [9].

The most common resistance sensors are sensors based on single semiconductor oxide materials, e.g. such as TiO_2 or SnO_2 [10]. Each of these oxides has its good and bad properties. Their combination can eliminate what affects unfavourably detection measurements, but at the same time it can help to obtain better sensing readings, including good sensitivity at low and high temperatures, and increase selectivity on particular gases, e.g. NH_3. In case of ammonia detection, the detection mechanism is complex, because reduction process of NH_3 occurring on the sensor surface results in NO_x oxides (oxidizing gases), which makes it difficult to measure when e.g. sensors on the basis of only TiO_2 are used. Sensor on the basis of TiO_2 is sensitive to both NH_3 and NO_x, which does not give a reliable result, and therefore only an addition of SnO_2 to the layout (which does not react with NO_x) enables reliable ammonia detection [10–13]. The aim of this work was to make TiO_2-SnO_2 nanocomposites. The effect of composition of nanocrystalline TiO_2-SnO_2 on the sensor dynamic responses to NH_3 has been examined. The synthesis of such material is important to achieve the best performance of nanosensors.

II. Materials and methods

2.1. Preparation of TiO_2-SnO_2 nanocomposites

Nanocomposites TiO_2-SnO_2 with different SnO_2 amounts (e.g. 26.9, 58.7 and 79.0 wt.% - the samples denoted TS-27, TS-59, TS-79 respectively) were obtained by a two-stage sol-gel method based on hydrolysis reactions.

In the first synthesis stage, nanocrystalline TiO_2 was received in such a way that up to 580 ml of isopropyl alcohol, HCl (36%) and CH_3COOH (27%) were mixed in order to obtain pH ~ 3. Then 58 ml of TIP (titanium (IV) isopropoxide, 98%) was added to the solution, mixed and added to 464 ml of distilled water. The resulting titanium hydroxide gel was dried at 115 °C for 18 h and calcined at 500 °C for 2 h. The calcination temperature was determined based on the results of TG/DSC analysis (Fig. 1). The calcined TiO_2 powder was ground in a mortar.

The second stage of nanocomposites TiO_2-SnO_2 synthesis consisted of introduction of SnO_2 nanoparticles. For this purpose, an appropriate amount of $SnCl_4$ (99%) was diluted ten times in distilled water at room temperature and instilled to colloidal solution. The colloidal solution was prepared by ultrasonic dispersion of 2 g of the obtained TiO_2 nanopowder in aqueous solution of NH_4OH (60 ml NH_4OH (25%) dissolved in 160 ml of distilled water) with constant mixing (in order to receive SnO_2, only NH_4OH solution was used). The suspensions were then dried in a laboratory drier at 115 °C for 18 h and calcined at 400 °C for 1 h. The calcination temperature was determined based on results of TG/DSC analysis (Fig. 2).

2.2. Characterization methods

Calcination and phase transition temperatures were determined on the basis of thermogravimetry and differential scanning calorimetry (TG/DSC) using Netzsch

STA 449 F3 apparatus. The study was conducted at temperature range of 25–825 °C using a heating rate of 10 °C/min. The samples in a form of hydroxide gels were prepared for the study.

In order to carry out qualitative and quantitative analyses of the obtained nanopowders, the powder X-ray diffraction method was applied using X'Pert Pro of PANalytical Company, operating in Bragg-Brentano configuration, with 2θ angle of 10–70° and 0.008° step. For measurements Cu lamp with Ni filter with λ = 0.1546 nm radiation wavelength was used. Interpretation of diffractograms was carried out using the Rietveld method.

Measurements of powder specific surface area were conducted using low temperature nitrogen adsorption and Brunauer-Emmett-Teller (BET) method. Samples of powders with a mass of about 0.2 g were degassed at 110 °C for 3 h. The adsorption measurements were conducted in relative pressures (P/P_s) from 0.01 to 1. Measurements were conducted using NOVA 1200e of Quantachrome Instruments Company.

The average particle sizes (D_{BET}) of TiO_2 and SnO_2 powders were also estimated on the basis of the specific surface area (S_w) and density (ρ) using dependence $D_{BET} = 6000/(\rho \cdot S_w)$ [14].

For morphology examinations, nanopowders were applied on copper micromesh and observed using the transmission electron microscope (TEM) TECNAI FEG f-my FEI at 200 kV acceleration voltage. This microscope was also used to determine the actual position of atoms in the dark field of vision obtained with scanning and transmission technique STEM-HAADF combined with EDS microanalysis that enabled identification of chemical elements contained in the studied material. By observing materials using the high resolution transmission electron microscope (HRTEM) and analysing distribution of atomic planes, individual particles of powders and interphase boundaries were also detected.

2.3. Gas sensing test

Sensor properties of the obtained composite materials for NH_3 gas detection were determined with thermostimulated conductance (TSC) method. Changes of current in the sensor at a constant voltage of 2 V were measured during cyclical changes in the radiator temperature from 200 °C up to 750 °C (heater temperature was changed at a rate of 2 °C/s). During measurements, the sensor was placed in a measuring chamber containing a precisely defined gas atmosphere (500–4000 ppm NH_3 or laboratory air as a reference atmosphere). The final changes in conductance of the active layer have been determined using the Ohm's law ($R = U/I$, where R is resistance, U is voltage and I is current) [15].

The studied gas sensor was made using thick layers of aluminium oxide substrate (96% Al_2O_3) with a thickness of 250 μm and an area of 25.40×2.45 mm. ESL-403 of ESL Europe Company was used to prepare pastes. The paste with a given material was printed on the substrate and dried first at room temperature, then heated at 400 °C for 10 minutes. On one side of the substrate, golden electrodes were made with an area on gas-soil layer in the upper part of substrate (distance between electrodes was 200 μm). On the other side of substrate, there was a meander-shaped platinum radiator with an area of 7.10 mm^2. The value of measurement signal (S, sensitivity of sensors) was determined as a function of temperature for different concentrations of NH_3 using G/G_{air} relation, where $G = 1/R$ indicates conductance in the presence of NH_3, while G_{air} indicates conductance measured in the reference atmosphere, that is laboratory air (20 °C, 45% humidity).

III. Results and discussion

3.1. Characterization of TiO_2-SnO_2 nanocomposites

The calcination temperature of titanium hydroxide was determined based on the results of TG/DSC analysis, which was conducted for titanium hydroxide gel (Fig. 1). Two clear ranges of mass loss can be defined on TG curve. The first mass loss (13.41%) at about 250 °C is associated with the loss of excess water and occluded solvent. In this temperature range, on DSC curve weak local endothermic minima is visible. The second stage of weight loss (7.08%) is between 250 °C and

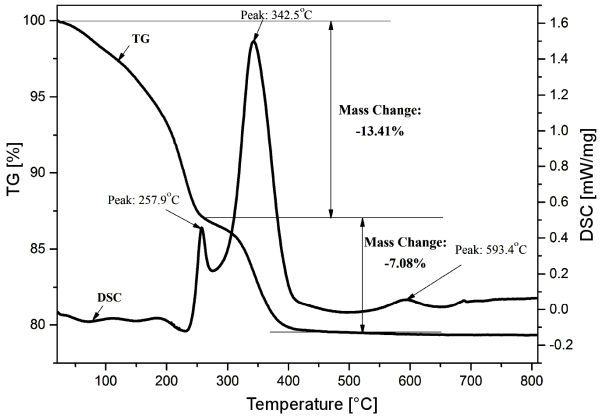

Figure 1. TG/DSC analysis of titanium hydroxide gel

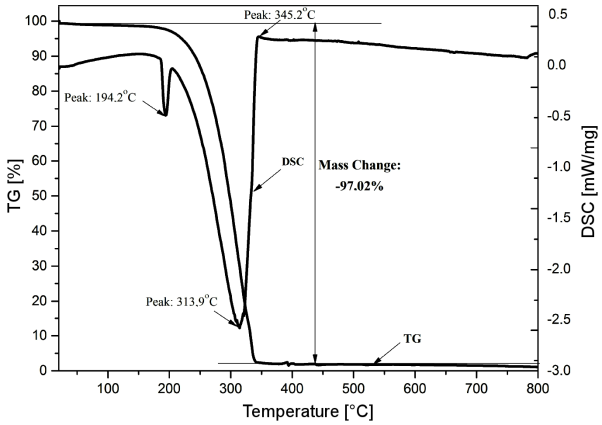

Figure 2. TG/DSC analysis of tin hydroxide gel

400 °C. DSC curve shows two local exothermic maxima (257.9 °C and 342.5 °C) associated with heat generation due to the combustion of decomposition products of titania precursor as well as with secretion of H_2O produced during hydroxide decomposition. The change of enthalpy on DSC curve at 593.4 °C is probably due to the phase transition of anatase into rutile.

In order to obtain nanocrystalline composites TiO_2-SnO_2, SnO_2 nanoparticles were introduced into the layout through calcination of tin hydroxide gel. The calcination temperature was determined based on results of TG/DSC analysis (Fig. 2). A large loss of mass (97.02%) up to about 350 °C is due to the loss of excess water and occluded solvent, removal of NH_4Cl decomposition products, as well as secretion of H_2O produced during hydroxide decomposition. Two distinct endothermic signals (194.2 °C and 313.9 °C) are visible on DSC curve in the discussed temperature range. The heat associated with decomposition of $Sn(OH)_4$ is greater than the heat of SnO_2 crystallization, and therefore no exothermic effect is observed on DSC curve.

Phase composition of the calcined nanocomposites TiO_2-SnO_2, mass proportions of both oxides and average values of crystallites determined by XRD (Fig. 3) were presented in Table 1. It is obvious that SnO_2 is much smaller than TiO_2 crystallites. Table 1 also shows measured values of specific surface areas. An example of isotherm for the pure SnO_2 nanopowder is shown in Fig. 4. The specific surface area of the pure titanium(IV) oxide powder is the lowest (only 42.1 m^2/g). With the increase in SnO_2 content in composite, the specific surface area increases as a result of the increasing number of smaller particles.

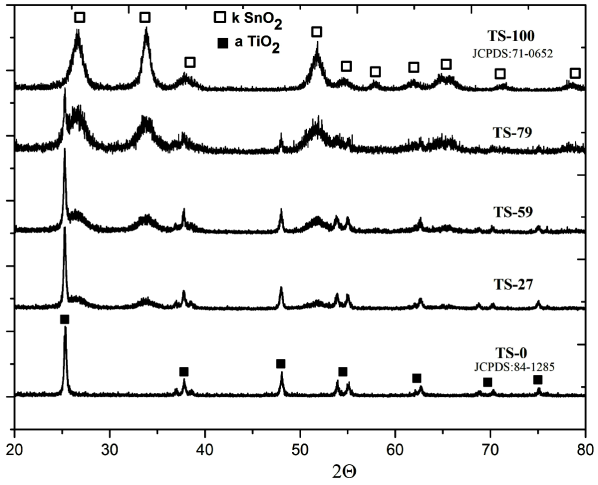

Figure 3. XRD diffractograms of the calcined nanopowders

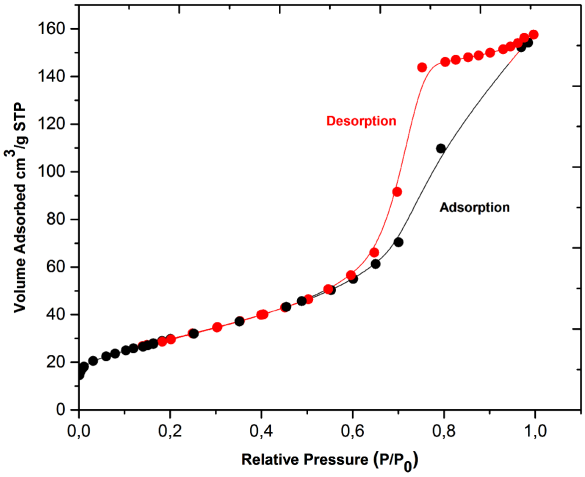

Figure 4. BET isotherms for SnO_2 nanopowder (sample TS-100)

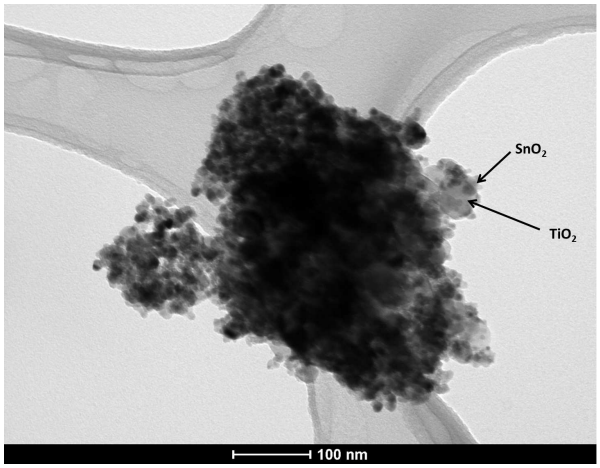

Figure 5. TEM microphotographs of calcined TS-79 powder

The morphology of the nanocomposites was observed with transmission electron microscope TEM (Fig. 5). The analysis showed the presence of particles diversified in terms of size similar to sizes of crystallites determined with X-ray diffraction. The smaller size of SnO_2 nanoparticles is caused by a lower calcination temperature as well as the formation of nucleation seeds on the surface of TiO_2 grains. Due to the large increase of the surface area (and thus high surface energy), nanometric particles are subject to considerable agglomeration, but the created aggregates are quite loose.

Table 1. Selected properties of calcined powders: phase mass fractions (a-TiO_2 anatase, k-SnO_2 cassiterite), the average crystallite size (D_{hkl}) determined by XRD and specific surface area (S_w) and average partcle size (D_{BET}) estimated by BET

Sample no.	Calcination temperature [°C]	Mass fractions of k-SnO_2 [%]	D_{hkl} of a-TiO_2 [nm]	D_{hkl} of k-SnO_2 [nm]	S_w [m^2/g]	D_{BET} [nm]
TS-0	500	0	24.0 ± 0.2	-	42.1 ± 5.2	37.5 ± 1.2
TS-27	400	26.9	24.0 ± 0.2	3.3 ± 0.2	75.4 ± 5.2	
TS-59	400	58.7	24.0 ± 0.2	3.3 ± 0.2	81.8 ± 5.2	
TS-79	400	79.0	25.0 ± 0.2	3.3 ± 0.2	100.6 ± 5.2	
TS-100	400	100	-	3.3 ± 0.2	160.8 ± 5.2	5.4 ± 1.2

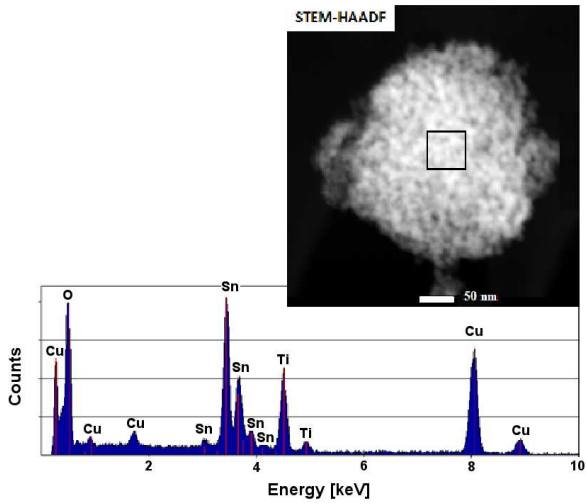

Figure 6. STEM-HAADF images of calcined TS-79 powder (62.3% Sn, 25.1% O, 12.6% Ti) with EDS spectrum of the selected area

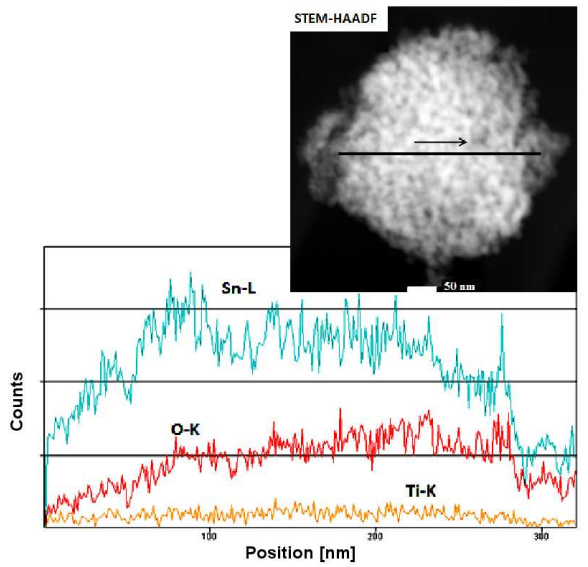

Figure 7. STEM-HAADF images of calcined TS-79 powder with EDS spectrum of the linear analysis

In order to confirm the chemical composition of powders, EDS analyses were carried out. Examples of EDS spectra from selected area and linear analysis of the sample TS-79 are presented in Figs. 6 and 7, respectively. The linear analysis also confirmed that the obtained composite nanopowders form agglomerates in the structure of material.

The high-resolution transmission electron microscope (HRTEM) was used to observe the crystalline structure of powders in small areas. Analysing the distribution of atomic surfaces, individual particles of powders were identified. Figure 8 shows the crystalline anatase in TS-79 powder (interstitial distance for crystallographic orientation of 111 anatase planes is d_{111} = 3.49 Å). However, Fig. 9 shows the crystalline cassiterite in the same composite powder (distance between surfaces for crystallographic orientation of 101 cassiterite planes is d_{101} = 2.654 Å).

3.2. Sensor properties of TiO_2-SnO_2 nanocomposites

Sensor properties for NH_3 gas detection of the TiO_2-SnO_2 composite materials were also investigated and compared with properties of the pure TiO_2 and SnO_2. The measurements were conducted at different NH_3 concentrations of 500, 1000, 2000 and 4000 ppm in reference atmosphere (laboratory air) in 200–750 °C temperature range. Figure 10 shows graphs of conductance temperature changes ($G = 1/R$) for sensors made of the calcined samples. Changes in conductance are caused by changes of NH_3 concentration in the air. An increase in conductivity of gas-sensitive layer caused by the addition of ammonia to the test atmosphere (which is characteristic for reducing gases) was observed. Disturbances on graphs below 350 °C result to the effect of humidity on the sensor response.

In the case of the sensors made of TiO_2, as well as nanocrystalline TiO_2-SnO_2 composites differences in the conductance values caused by changes in NH_3 concentration at low temperatures (less than 400 °C) are not observed. Only above 400 °C measured conductance values can be precisely correlated with the ammonia concentration (Fig. 10b,c,d). Below 400 °C, the mate-

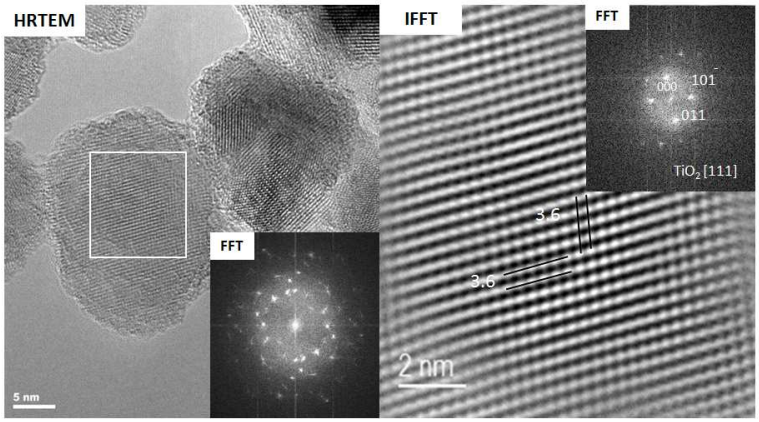

Figure 8. HRTEM images of calcined TS-79 powder showing crystalline TiO_2-anatase (left image - HRTEM with fast Fourier transform (FFT), right image - fast Fourier transform and inverse fast Fourier transform (IFFT))

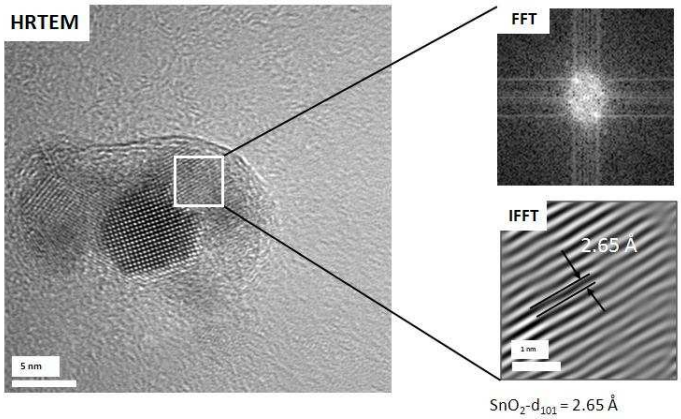

Figure 9. HRTEM images of calcined TS-79 powder showing crystalline SnO_2-cassiterite (left image - HRTEM, right image - fast Fourier transform (FFT) and inverse fast Fourier transform (IFFT))

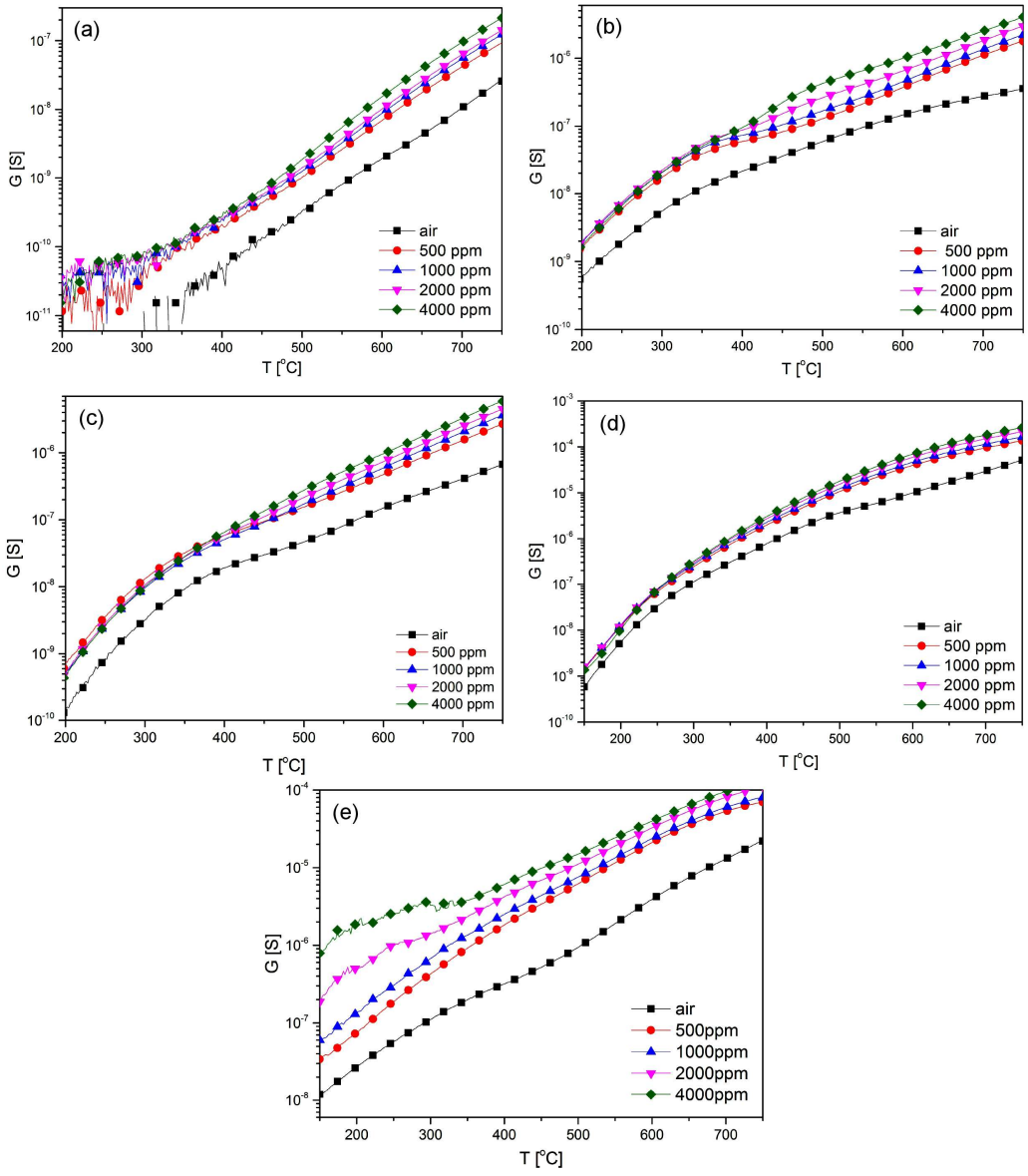

Figure 10. Temperature changes of the sensor conductance of samples: a) TS-0, b) TS-27, c) TS-59, d) TS-79 and e) TS-100

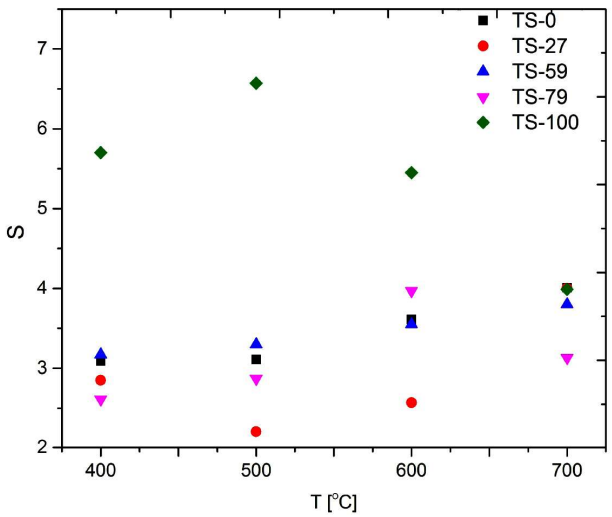

Figure 11. Dependence of sensor sensitivity as a function of temperature at 500 ppm of NH_3 in laboratory air

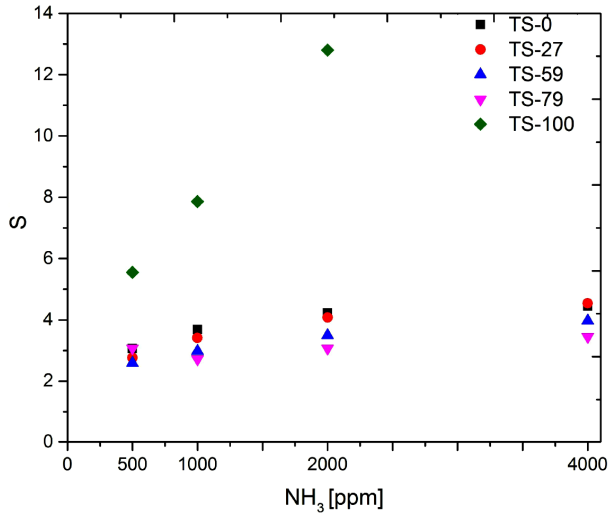

Figure 12. Dependence of sensor sensitivity as a function of NH_3 concentration at 400 °C

rials are sensitive to NH_3, but regardless of ammonia concentration, the sensors do not show any changes typical for gas-sensitive materials. However, in the case of SnO_2 sensor, a systematic increase in the conductance value is observed along with the increase of NH_3 concentration over the entire temperature range (Fig. 10e).

Figure 11 shows the influence of temperature on the value of measurement signal (sensitivity, $S = G/G_{air}$) of sensors for selected NH_3 concentration (500 ppm) in the reference atmosphere, i.e. laboratory air. The first observation concerns the difference of the response curve vs. temperature for TS-100 sample with respect to all the other sensors. Indeed, while response versus temperature of TS-100 sample exhibited a bell-shaped curve, but the responses of all the other sensors increased with the increase of temperature. The increase in temperature accelerates the gas reaction with the surface of the sensor thus increasing its sensitivity. However, deterioration of these properties with an increase in temperature can be observed in the case of TS-100 sensor (Fig. 11). The addition of SnO_2 to the pure TiO_2 improves the measurement signal G/G_{air} for the presence of ammonia in air, which increases along with the increase of temperature.

In the case of TiO_2-SnO_2 nanocomposites, direct contact between the grains creates an area where a band bending complex and charge transfer from TiO_2 to SnO_2 can be observed, since the maximum and the minimum of the conduction band in TiO_2 is above the corresponding bands in SnO_2. The situation of energy levels results in translocation and separation of excited electron carriers, which increases the response of gas sensors based on this type of materials. This is because in reality, initial gas adsorption on the surface of a grain is substantially greater at proper electron concentration. It is usually assumed that SnO_2 grains are more suitable for oxygen adsorption, and hence electron transfer from TiO_2 grains to SnO_2 grains is necessary for increasing the number of adsorption, and thus increasing the sensor response. The difference of potentials formed as a result of contact between TiO_2 and SnO_2 grains facilitates electron transport from TiO_2 to SnO_2, which accelerates initial adsorption of oxygen on the surface of SnO_2 grains. Moreover, the smaller the size of grains, the greater the potential difference, and hence, the greater sensor response [8,16,17].

The responses of all sensors with respect to 500, 1000, 2000 and 4000 ppm of ammonia in dry air at 400 °C are shown in Fig. 12. Both the sensor made of TiO_2 and nanocrystalline TiO_2-SnO_2 composites show the increase in sensitivity ($S = G/G_{air}$) along with the increase in analysed gas concentration at 400 °C for all NH_3 concentrations.

The investigated nanocomposites are characterised by very good NH_3 detection properties compared to materials described in other papers. Radecka *et al.* [5] describe a sensor built using material that contained 50% SnO_2 and 50% TiO_2, which manifested the highest sensitivity to NH_3 (1200 ppm) at 400 °C $R/R_0 = 1.49$. Its sensitivity decreased for lower ammonia concentrations. In turn, for a sensor described in a study by D.H. Kim *et al.* [18], built using composite material in the form of thin layers (the SnO_2 layer on the surface of TiO_2) sensitivity was $S = 2$ at 400 °C and NH_3 pressure 1000 ppm. The sensor TS-59 built using the material described in this study achieved a far better value of sensitivity, i.e. $S = 3.7$, under the same conditions of pressure and temperature. Thus, these sensors can be used to prevent the escape of ammonia gases to the atmosphere during the production of nitric acid at elevated temperatures.

IV. Conclusions

This work describes the production of nanocrystalline TiO_2 and SnO_2 oxides, as well as their nanocomposites (containing 26.9, 58.7 and 79.0 wt.% of SnO_2) with two-stage sol-gel method combined with high temperature treatment. The prepared samples are well crys-

tallized and consist of anatase TiO_2 and cassiterite SnO_2 spherical nanograins.

Sensors made of TiO_2-SnO_2 nanocomposites show a systematic increase in conductance along with the increase in NH_3 concentration above 400 °C, as well as a high sensitivity (G/G_{air}) for the presence of this gas. The addition of SnO_2 to the pure TiO_2 correlates the conductance values with NH_3 concentrations above 400 °C, and also improves G/G_{air} measurement signal for the presence of ammonia in air. The sensor with 58.7 wt.% of SnO_2 has a systematic increase in the value of conductance along with the increase of NH_3 concentration in the entire temperature range, as well as high sensitivity, which allows detection of very low NH_3 concentrations. This makes such material very promising for use as gas sensing element for ammonia sensors.

Acknowledgement: This work was supported financially by the National Science Centre (NCN) based on the decision number DEC-2015/19/N/ST8/00187. Support was also given from the Polish Ceramic Society. The authors thank to Prof. Bućko for executing X-ray diffraction analyses.

References

1. A. Hulanicki, S. Głab, F. Ingman, "Chemical sensors: Definitions and classification", *Pure Appl. Chem.*, **63** [9] (2009) 1247–1250.
2. A. Marzec, A. Kusior, M. Radecka, Z. Pędzich, "Preparation of nanocrytalline composites TiO_2-SnO_2 by sol-gel method", *Compos. Theory Pract.*, **14** [3] (2014) 169–173.
3. C. Altavilla, E. Ciliberto, *Inorganic Nanoparticles: Synthesis, Applications and Perspectives*, CRC Press Taylor & Francis Group, Boca Raton, 2010.
4. W.J., Moon, J.H. Yu, G.M. Choi, "Selective gas detection of SnO_2-TiO_2 gas sensors", *J. Electroceram.*, **13** (2004) 707–713.
5. M. Radecka, A. Kusior, A. Lacz, A. Trenczek-Zając, B. Łyson-Sypień, K. Zakrzewska, "Nanocrystalline TiO_2/SnO_2 composites for gas sensors", *J. Therm. Anal. Calorim.*, **108** (2012) 1079–1084.
6. A. Szczurek, *Pomiary lotnych związków organicznych rezystancyjnymi czujnikami gazów*, Oficyna Wydawnicza Politechniki Wrocławskiej, Wrocław, 2006.
7. L. Hozar, *Półprzewodnikowe materiały ceramiczne z aktywnymi granicami ziarn*, Państwowe Wydawnictwo Naukowe, Warszawa, 1990.
8. B. Lyson-Sypien, A. Kusior, M. Rekas, J. Zukrowski, M. Gajewska, K. Michalow-Mauke, T. M. Graule, M. Radecka, K. Zakrzewska, "Nanocrystalline TiO_2/SnO_2 heterostructures for gas sensing", *Beilstein J. Nanotechnol.*, **8** (2017) 108–122.
9. B. Timmer, W. Olthuis, A. Berg, "Ammonia sensors and their applications review", *Sensors Actuators B*, **107** (2005) 666–677.
10. S. Maldonado, E. Garcia-Berrios, M.D. Woodka, B.S. Brunschwig, N.S. Lewis, "Detectin of organic vapors and NH_3(g) using thin-film carbon black-metallophtalocyanine composite chemiresistors", *Sensors Actuators B*, **134** (2008) 521–531.
11. A. Lobnik, O.S. Wolfbeis, "Sol-gel based optical sensor for dissolved ammonia", *Sensors Actuators B*, **51** (1998) 203–207.
12. S. Khoby-Shendy, M.R. Vaezi, T. Ebadzadeh, "Synthesis of TiO_2/SnO_2 core shell nanocomposite via sol-gel method", *Int. J. Modern Phys. Conf. Conf. Ser.*, **5** (2012) 251–256.
13. W. Zeng, T. Liu, Z. Wang, "Sensitivity improvement of TiO_2-doped SnO_2 to volatile organic compounds", *Physica E*, **43** (2010) 633–638.
14. P. Radomski, A. Jarosiński, "Determination of specific surface area of the granular materials in aspect of its use in selected technological processes", *Tech. Trans. Cracow Univ. Techn.*, **10** (2010) 267–276.
15. F.T. Brown, *Engineering System Dynamics: A Unified Graph-Centered Approach*, CRC Press, 2006 (p. 43).
16. M.C. Carotta, S. Gherardi., V. Guidi, C. Malagù, G. Martinelli, B. Vendemiati, "Electrical and spectroscopic properties of $Ti_{0.2}Sn_{0.8}O_2$ solid solution for gas sensing", *Thin Solid Films*, **517** (2009) 6176–6183.
17. K. Zakrzewska, M. Radecka, "TiO_2-SnO_2 composites and solid solutions for chemical nanosensors", *Procedia Eng.*, **47** (2012) 1077–1080.
18. D.H. Kim, W.S. Kim, S.B. Lee, S.H. Hong, "Gas sensing properties in epitaxial SnO_2 films grown on TiO_2 single crystals with various orientations", *Sensors Actuators B*, **147** (2010) 653–659.